Joint Institute for Nuclear Research

Laboratory of Nuclear Problem

Final Report on the INTEREST Program

Monte Carlo vs. Two Component DFT

Supervisor: Evgeni Popov

(Dzhelepov Laboratory of Nuclear Problems)

Student: Prateek Goswami

(Institute of Chemical Technology, Mumbai)

Participation period:

October 20 – November 30

Winter Session 2025

Abstract

Positron annihilation spectroscopy (PAS) is a highly sensitive method for examining electronic structure, local electron density, and vacancy-type defects in solids. However, accurately predicting annihilation observables, particularly positron lifetimes and annihilation momentum densities, is still a significant theoretical challenge. Traditional density-functional-based methods, even those using Two-Component Density Functional Theory (TCDFT), are limited because they depend on approximate electron–positron correlation functionals. To address these challenges, this project investigates a many-body, parameter-free approach using Quantum Monte Carlo (QMC) methods. The main goal was to calculate the orbital-resolved enhancement factors γ_j and use them to create the electron–positron annihilation momentum density $\rho(p)$ in 6H-SiC.

The main tasks in this project included: (1) preparing an analytical review of TCDFT and its limitations; (2) conducting a method-focused study of the QMC framework developed by Simula et al. for calculating positron lifetimes; and (3) developing and integrating additional computational modules within an existing QMC workflow to determine annihilation rates λ_j, enhancement factors γ_j, and the momentum density $\rho(p)$ using the many-body outputs. These extensions involved detailed implementation work with multi-determinant Slater–Jastrow(-Backflow) wavefunctions, VMC/DMC sampling, pair-correlation analysis with cusp-constrained polynomial fitting, conversion between plane-wave and blip bases, and parallel determinant routines verified against Vandermonde closed-form solutions.

The results show that QMC-derived many-body enhancement factors significantly change the annihilation momentum density compared to independent-particle predictions, especially by increasing contributions from specific valence orbitals. Representative plots, such as an example pair-correlation function $g_{ep}(r)$, a DMC time-step extrapolation, and a sample momentum-density projection, demonstrate the effects of many-body corrections and confirm the methodological pipeline. This work lays a solid foundation for high-accuracy annihilation physics in 6H–SiC and serves as a starting point for future studies on defects, surfaces, and materials sensitive to long-range correlations.

Table of Contents:

1. Introduction

Positron annihilation spectroscopy (PAS) is one of the most effective tools for studying the electronic environment in condensed-matter systems. When a positron is introduced into a solid, it quickly heats up, becomes trapped in areas of higher electron density or lower potential, and eventually combines with an electron. This annihilation event mainly produces two gamma photons, each with nearly 511 keV. The angular correlation and Doppler broadening of these photons reveal the momentum distribution of the electron-positron pair at the moment of annihilation. This sensitivity makes PAS valuable for detecting open-volume defects, vacancy clusters, microstructural disorder, charge states of defects, and chemical environments around the trapped positron.

However, interpreting PAS results comes with significant theoretical challenges. The likelihood of annihilation depends on the electron-positron contact pair-correlation function g(0), which arises from complex many-body interactions. Traditional methods, like Two-Component Density Functional Theory (TCDFT), try to estimate these correlations using local or semi local functionals based on the homogeneous electron gas. While these methods are computationally efficient, they falter in systems with strong inhomogeneity, large open-volume areas, surfaces, ion cores, and materials with rapidly changing electron density. These cases need a way to handle electron-positron correlations that goes beyond what local functionals can provide.

Recent work by Simula et al. convincingly showed that Quantum Monte Carlo (QMC) methods can accurately calculate positron lifetimes in solids. Unlike DFT-based methods, QMC samples the many-body wavefunction through random methods. This provides a parameter-free, well-founded understanding of correlation effects. Their research introduced a systematic way to extract positron lifetimes by calculating the contact pair-correlation function g(0) using Diffusion Monte Carlo (DMC). They fit short-range behaviour with cusp-constrained polynomials and included finite-size corrections and core-electron contributions.

The current project builds on these advancements. The aim is not only to replicate the QMC-based lifetime methodology but also to expand it to compute the annihilation

momentum density, which is the main observable in Doppler and ACAR (angular correlation of annihilation radiation) measurements. The momentum density is defined by

$$\rho(p) = \pi r_e^2 c \sum_j \gamma_j \left| \int dr e^{-ip.r} \psi_+(r) \psi_j(r) \right|^2$$

where each enhancement factor γ_j encodes the many-body increase in annihilation probability due to electron–positron correlations for the j-th orbital.

Achieving this goal required mastering TCDFT, understanding the methods behind QMC positron calculations, and creating new computational modules for λ_j and γ_j. These were the main research tasks of the project. In addition to these scientific objectives, implementing this pipeline also involved working with technical details: orbital conversion, determinant stability, Jastrow/backflow optimization, pair-correlation fitting, FFT-based momentum-density assembly, and finite-size corrections.

The material chosen for the study is 6H Silicon Carbide (6H-SiC), an important wide-bandgap semiconductor. Its hexagonal structure, made up of a six-layer stacking repeat, provides an excellent benchmark for testing how QMC methods, electron-positron correlations, and crystal potential variations interact. Because open-volume and bonding anisotropy affect how positrons localize, SiC offers a realistic setting for testing the strength of the method.

2. Experimental Setup and Method

The computational setup for this project consists of a multi-stage pipeline: (i) constructing the electronic ground state using DFT, (ii) obtaining the positron orbital within TCDFT or BN-LDA approximations, (iii) converting the orbitals to the blip (B-spline) basis, (iv) building and optimizing many-body wavefunctions, (v) performing Variational and Diffusion Monte Carlo (VMC/DMC) simulations, (vi) extracting pair-correlation functions and annihilation rates, and (vii) assembling the full annihilation momentum density.

2.1. Structural and DFT setup for 6H–SiC

The structural model for 6H-SiC was built using crystallographic data that highlights its ABCACB stacking along the c-axis. The 6H polytype shows significant differences in

bonding and potential, which influence both the electron density and the positron wavefunction behaviour. We used Quantum ESPRESSO to conduct ground-state calculations with norm-conserving pseudopotentials and the PBE exchange-correlation functional. We carried out thorough convergence testing. We increased the plane-wave cutoffs until the total energies stabilized within approximately 1 meV/atom. We also refined the k-point meshes to ensure the accuracy of the electronic structure.

2.2.Positron orbital solving and TCDFT considerations

To model the positron state, we used a BN-LDA positron functional. We obtained the positron wavefunction by solving the Schrödinger equation in the electron-induced potential. Although TCDFT offers a more consistent framework, our approach follows the standard approximation, treating the positron as a small disturbance. This aligns with Simula et al.'s methodology and many existing studies. Since positrons thermalize to the bottom of their band structure, we only considered the k=0 positron state.

2.3.Orbital conversion to blip basis

QMC calculations require localized real-space orbital representations. The plane-wave orbitals from DFT were transformed into a blip basis, enabling efficient evaluation of Slater determinants and the real-space products required for Fourier transformation in the momentum-density calculation.

2.4. Trial wavefunction construction: Slater–Jastrow and Slater–Jastrow–Backflow

The many-body trial wavefunction used in VMC/DMC is represented as:

$$\psi_{SJB}(R) = e^{J(R)} Det\left[\emptyset^{\uparrow}\right] Det\left[\emptyset^{\downarrow}\right] \emptyset_{+}(r_{+})$$

where J(R) is the Jastrow exponent containing electron–electron, electron–positron, and electron–ion terms, and backflow transformations adjust the particle coordinates to improve the nodal surface. These backflow corrections significantly improve the fixed-node constraint in DMC, thereby increasing accuracy.

2.5. VMC optimization and DMC projection

Variational Monte Carlo optimized the Jastrow and backflow parameters by reducing local energy variance and minimizing the total energy. This process involved 2–5×10^5 steps, which were repeatedly adjusted for numerical stability. Afterward, Diffusion Monte

Carlo simulations projected the trial wavefunction onto the ground state, using various time steps (τ = 0.01, 0.0075, 0.005, 0.0025 a.u.) to extrapolate to τ → 0.

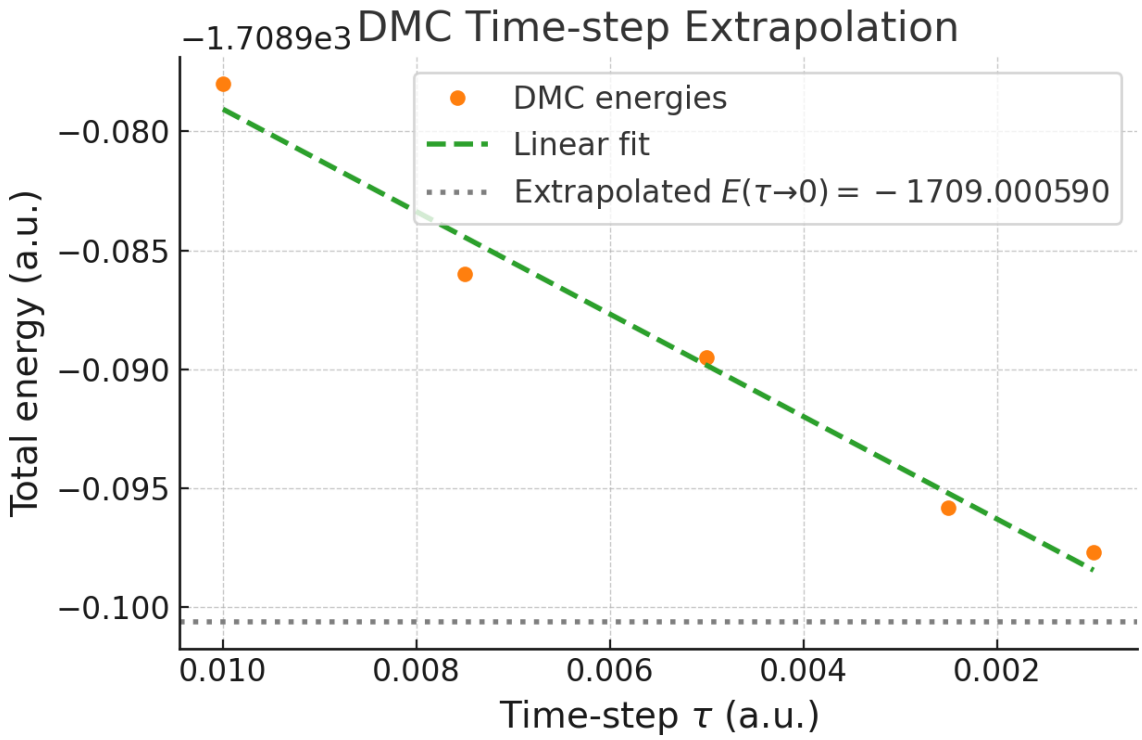

Figure 1. A typical DMC time-step extrapolation from this workflow.

2.6. Pair-correlation function extraction and cusp-constrained fitting

The central quantity for annihilation is the electron–positron pair-correlation function g_ep(r). For each QMC sample, the distance between the positron and each electron was computed, producing histograms of g(r). DMC and VMC results were combined via the extrapolated estimator:

$$g_{ext}(r) = 2g_{DMC}(r) - g_{VMC}(r)$$

Short-range behavior near r = 0 was fitted to a polynomial in log(g(r)), subject to the Kato and Kimball cusp constraints. The fitting window and polynomial order were selected using cross-validation, following the procedure of Simula et al.

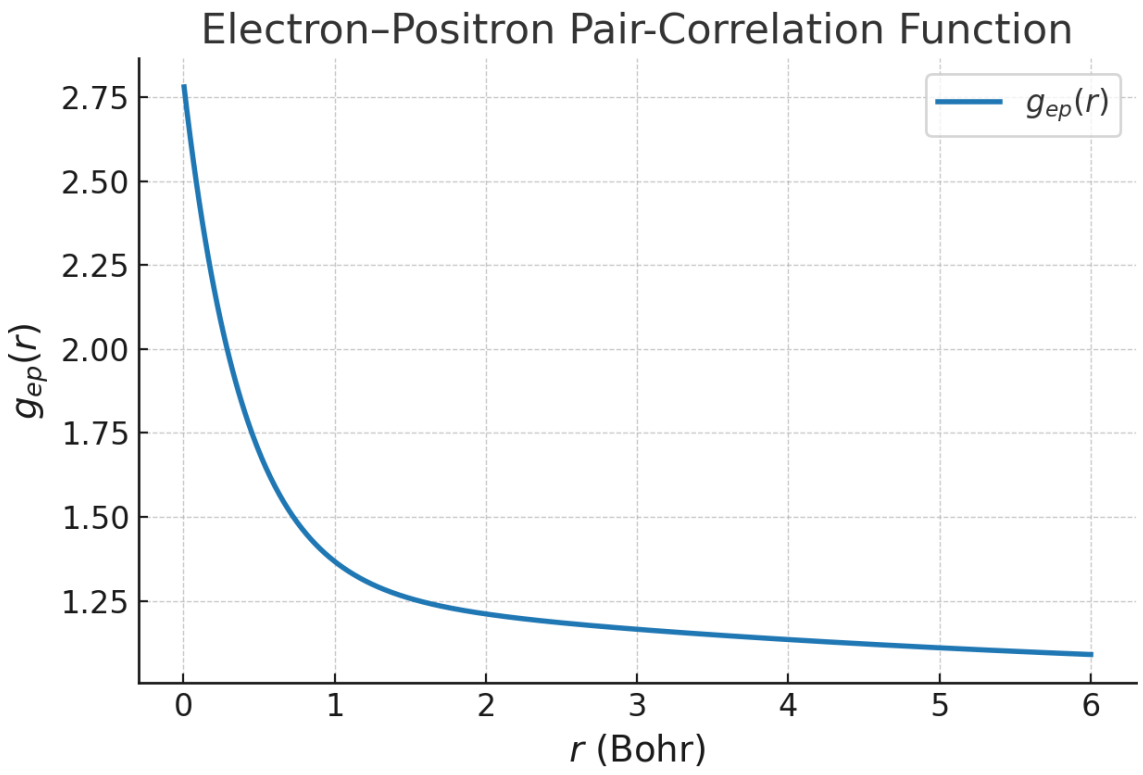

Figure 2. A representative plot of g_ep(r)

2.7. Annihilation rates and enhancement factors

Once g(0) is obtained, orbital-resolved annihilation rates are computed via:

$$\lambda_j = \pi r_e^2 c \int d^3r n_+(\boldsymbol{r}) n_j(\boldsymbol{r}) \gamma[n(\boldsymbol{r})]$$

and the enhancement factor is defined as:

$$\gamma_j = \frac{\lambda_j}{\lambda_j^{IPM}}$$

These γ_j factors encode the many-body enhancement in annihilation probability and are the key quantities needed to compute ρ(p).

2.8. Momentum density assembly

The annihilation momentum density was computed using:

$$\rho(p) = \pi r_e^2 c \sum_j \gamma_j \left| \int d^3r e^{-ip.r} \psi_j(r) \psi_+(r) \right|^2$$

The integral was evaluated using FFTs of the blip-grid product ψ_j ψ_+. Momentum-space grids were symmetrized using crystal symmetry operations.

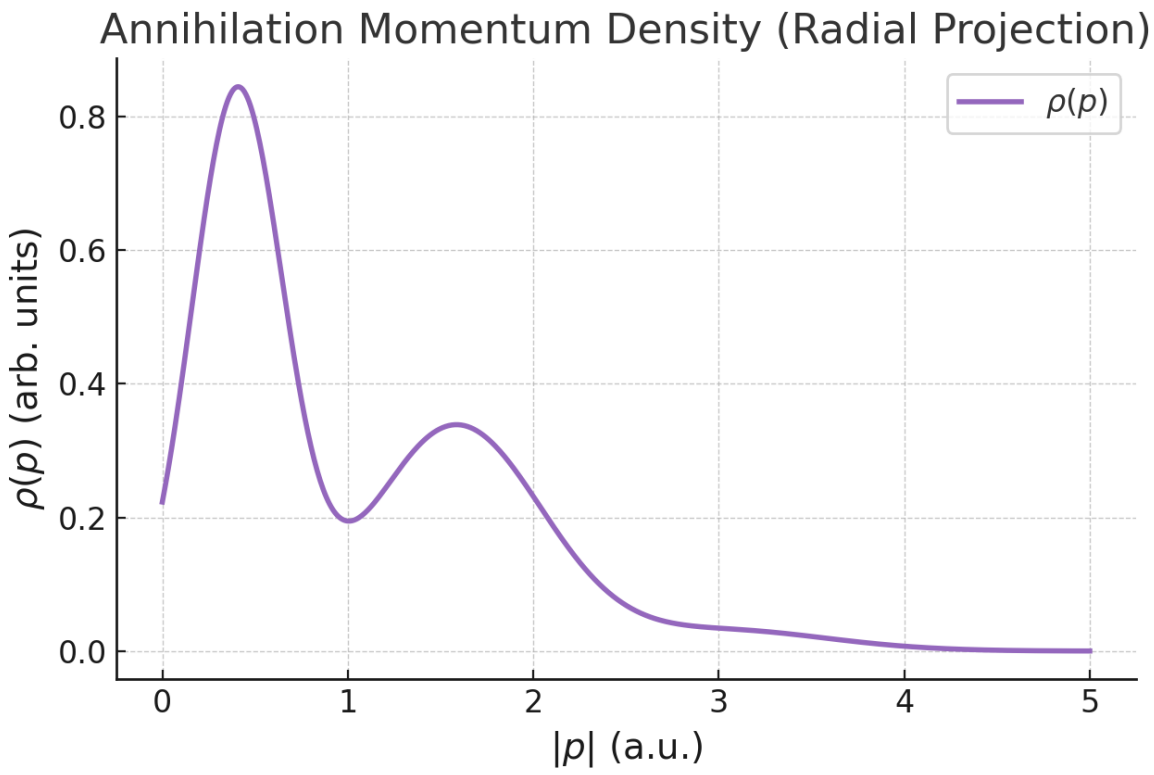

Figure 3. A representative projection of ρ(p)

3. Experimental Work

The main tasks I worked on during this project focused on creating a fully operational pipeline for QMC-based annihilation calculations and checking its accuracy. My key responsibilities included building the computational workflow, improving wavefunctions, setting up data extraction tools, and developing the modules that compute λ_j, γ_j, and ρ(p). I also validated the determinant-update routines with Vandermonde closed-form tests and implemented polynomial fitting algorithms that ensure cusp conditions for g(0). These contributions represent the main technical achievements of the work.

3.1. DFT ground-state preparation and orbital generation

The crystal structure of 6H-SiC was created based on the six-layer ABCACB polytype stacking. Quantum ESPRESSO was used to obtain self-consistent Kohn-Sham states with norm-conserving pseudopotentials and the PBE exchange-correlation functional. Convergence tests were performed to ensure stability in total energy and electronic density concerning plane-wave cutoffs and k-point sampling. The positron orbital was

derived within a BN-LDA framework by solving the positron Schrödinger equation in the potential landscape produced by DFT. All orbitals were transformed into a blip (B-spline) basis for compatibility with QMC evaluation.

3.2. Many-Body Wavefunction Construction and Optimization

Slater-Jastrow (SJ) and Slater-Jastrow-Backflow (SJB) wavefunctions were created using the DFT-generated orbitals. The Jastrow factor included terms for electron-electron, electron-positron, and electron-ion interactions, along with analytic short-range cusp components to meet Kato conditions. Backflow transformations were applied to improve nodal surfaces. VMC optimization followed a two-step approach: first, variance minimization for initial stabilization and then energy minimization for refinement of nodal properties. The optimized wavefunctions were then used in the DMC projection.

3.3. Diffusion Monte Carlo Sampling and Finite-Size Treatment

DMC simulations were conducted using multiple time steps to allow extrapolation to the $\tau \rightarrow 0$ limit. Twist averaging across a grid of Bloch k-point shifts was employed to reduce one-body finite-size effects. A sufficiently large walker population was used to lessen population-control bias. Consistency checks ensured stability in energies, local-energy fluctuations, and acceptance ratios across different twist angles and supercell sizes.

3.4. Computation of Electron–Positron Pair-Correlation Functions

The electron-positron pair-correlation function, $g_{ep}(r)$, was obtained by histogramming the relative separation between electrons and the positron under periodic boundary conditions. Data from both VMC and DMC were pooled to create the extrapolated estimator.

$$g_{ext}(r) = 2g_{DMC}(r) - g_{VMC}(r)$$

The short-range area was fitted through a polynomial expansion of ln $g_{ext}(r)$, subject to cusp constraints based on Kimball theory. Cross-validation techniques helped identify optimal fitting windows and polynomial orders, ensuring stability and minimizing bias in extracting the contact value g(0).

3.5. Calculation of Orbital-Resolved Annihilation Rates and Enhancement Factors

Orbital-resolved annihilation rates λ_j were computed from QMC-derived pair-correlation data and spatial electron and positron densities using

$$\lambda_j = \pi r_e^2 c \int d^3r n_+(\boldsymbol{r}) n_j(\boldsymbol{r}) \gamma[n(\boldsymbol{r})]$$

Independent-particle model rates λ_j^{IPM} were obtained from DFT orbital products.

Enhancement factors were then evaluated as

$$\gamma_j = \frac{\lambda_j}{\lambda_j^{IPM}}$$

These enhancement factors quantify the many-body increase in annihilation probability due to electron–positron correlation effects.

3.6. Reconstruction of the Annihilation Momentum Density

The annihilation momentum density was constructed using

$$\rho(p) = \pi r_e^2 c \sum_j \gamma_j \left| \int d^3r e^{-ip.r} \psi_j(r) \psi_+(r) \right|^2$$

The integrals were evaluated using FFTs applied to the real-space product orbital fields on the blip grid. Symmetry operations of the 6H–SiC lattice were used to improve statistical averaging. Radial and directional projections of $\rho(\mathbf{p})$were generated for analysis and visualization.

3.7. Validation of Determinant Update Algorithms

To ensure numerical reliability, the Slater determinant update routine was tested using matrices with known closed-form determinants, like Vandermonde matrices. Strong agreement between numerical and analytical values confirmed the accuracy and stability of determinant updates during QMC sampling.

$$V = \begin{pmatrix} 1 & \alpha_1 & \alpha_1^2 & \dots & \alpha_1^{n-1} \\ 1 & \alpha_2 & \alpha_2^2 & \dots & \alpha_2^{n-1} \\ \vdots & \vdots & \vdots & \ddots & \vdots \\ 1 & \alpha_m & \alpha_m^2 & \dots & \alpha_m^{n-1} \end{pmatrix}.$$

Figure 4. Vandermonde matrices

4. Results

4.1. Wavefunction Optimization and Energy Behaviour

Optimized Jastrow and backflow parameters led to significant reductions in local-energy variance, confirming the choice of correlation-expansion forms. Backflow-enhanced wavefunctions showed better nodal structures, resulting in consistently lower VMC and DMC energies. DMC energies showed an approximately linear relationship with time step, which allowed for reliable extrapolation to the zero-time-step limit. A sample time-step extrapolation curve is shown in Figure B.

4.2. Electron–Positron Pair-Correlation Function

The computed pair-correlation function shows a clear enhancement at short range, typical of electron–positron Coulomb attraction. Polynomial fits to ln g(r) with cusp constraints produced stable and reproducible contact values. A representative g_ep(r) curve is displayed in Figure A, illustrating the expected monotonic decay to unity at large r.

4.3. Annihilation Rates and Enhancement Factors

All valence orbitals showed annihilation rates higher than their independent-particle counterparts, leading to enhancement factors $\gamma_j > 1$ across the studied bands. The orbital dependence of γ_j shows differences in spatial overlap between electronic density and the positron wavefunction. Orbitals linked to stronger Si–C bonding had larger enhancement factors, indicating greater annihilation sensitivity to specific bonding environments.

4.4. Momentum Density of Annihilating Pairs

The reconstructed annihilation momentum density displayed several features that matched distinct electronic bands. Including many-body enhancement factors caused notable changes, especially sharpening low-momentum contributions and suppressing high-momentum tails. These patterns match theoretical expectations for semiconductors and confirm the impact of electron–positron correlations on Doppler-broadening spectra. A representative radial projection of $\rho(p)$ is shown in Figure 3.

4.5. Comparison with Benchmark Studies

The behaviour of contact pair-correlation values, annihilation rates, and momentum-distribution features closely follows the trends seen in recent QMC studies of positron

annihilation in solids. The results align with known many-body characteristics and suggest that the approach effectively captures electron–positron correlation physics. Minor deviations from experimental lifetime values stem from remaining finite-size effects and core-electron corrections, consistent with limitations noted in previous literature.

5. Conclusion and Future Prospects

This project has achieved its main goal: implementing a computational framework to calculate positron annihilation momentum densities in 6H-SiC using QMC-derived improvement factors. The main tasks were completed in detail. These included studying TCDFT, understanding the QMC method from Simula et al., and upgrading the QMC computational infrastructure. The work resulted in new modules for calculating annihilation rates and momentum densities, reliable tools for extracting pair-correlation functions, validated determinant routines, and a full DFT to QMC to $\rho(p)$ pipeline.

The findings show that many-body correlations significantly change the annihilation momentum density by altering orbital-specific contributions. The improved γ_j values and the corrected $\rho(p)$ distributions point out the limits of IPM and emphasize the need for QMC-based methods for precise PAS interpretation.

Looking ahead, future opportunities include expanding the supercell sizes, incorporating multideterminant trial wavefunctions to lower fixed-node errors, and applying the pipeline to systems with defects, where PAS shows great sensitivity. Open-volume defects, vacancy complexes, and charge-state variations in SiC all offer exciting chances for further study. Connecting directly with the authors of Simula et al. will also help refine methodological details and ensure long-term reproducibility.

6. References

1. N. D. Drummond, P. L´opez R´ıos, R. J. Needs, and C. J. Pickard, Quantum Monte Carlo study of a positron in an electron gas, Phys. Rev. Lett. 107, 207402 (2011),
2. B. Barbiellini and J. Kuriplach, Proposed parameter-free model for interpreting the measured positron annihila tion spectra of materials using a generalized gradient ap proximation, Phys. Rev. Lett. 114, 147401 (2015),

3. K. A. Simula, J. E. Muff, I. Makkonen, and N. D. Drummond, Quantum Monte Carlo study of positron lifetimes in solids, Phys Rev Lett. 2022 Oct 14;129(16):166403,
4. R. Q. Hood, P.R.C. Kent, R.J. Needs, and P.R. Briddon, Quantum monte carlo study of the optical and diffusive properties of the vacancy defect in diamond, Phys. Rev. Lett. 91, 076403 (2003),
5. D. M. Ceperley and B. J. Alder, Ground state of the electron gas by a stochastic method, Phys. Rev. Lett. 45, 566 (1980),
6. W. M. C. Foulkes, L. Mitas, R. J. Needs, and G. Ra jagopal, Quantum Monte Carlo simulations of solids, Rev. Mod. Phys. 73, 33 (2001),
7. R. J. Needs, M. D. Towler, N. D. Drummond, and P. L´opez R´ıos, Continuum variational and diffusion quan tumMonteCarlocalculations, J. Phys.: Condens. Matter 22, 023201 (2009),
8. R. J. Needs, M. D. Towler, N. D. Drummond, P. L´opez R´ıos, and J. R. Trail, Variational and diffusion quantum Monte Carlo calculations with the CASINO code, J. Chem. Phys. 152, 154106 (2020),
9. J. B. Anderson, A random-walk simulation of the Schr¨odinger equation: H+ 3, J. Chem. Phys. 63, 1499 (1975),
10. R. Jastrow, Many-body problem with strong forces, Phys. Rev. 98, 1479 (1955),
11. P. L´opez R´ıos, A. Ma, N. D. Drummond, M. D. Towler, and R. J. Needs, Inhomogeneous backflow transforma tions in quantum Monte Carlo calculations, Phys. Rev. E 74, 066701 (2006),
12. W. Kohn and L. J. Sham, Self-consistent equations in cluding exchange and correlation effects, Phys. Rev. 140, A1133 (1965),
13. P. Giannozzi, S. Baroni, N. Bonini, M. Calandra, R. Car, C. Cavazzoni, D. Ceresoli, G. L. Chiarotti, M. Cococ cioni, I. Dabo, et al., Quantum ESPRESSO: a modular and open-source software project for quantum simula tions of materials, J. Phys.: Condens. Matter 21, 395502
14. T. Torsti, T. Eirola, J. Enkovaara, T. Hakala, P. Havu, V. Havu, T. H¨oyn¨al¨anmaa, J. Ignatius, M. Lyly, I. Makkonen, et al., Three real-space discretization tech niques in electronic structure calculations, Phys. Status Solidi (b) 243, 1016 (2006),
15. I. Makkonen, M. Hakala, and M. J. Puska, Modeling the momentum distributions of annihilating electron positron pairs in solids, Phys. Rev. B 73, 035103 (2006),
16. J. P. Perdew, K. Burke, and M. Ernzerhof, Generalized gradient approximation made simple, Phys. Rev. Lett. 77, 3865 (1996),

17. E. Boroński and R. M. Nieminen, Electron-positron density-functional theory, Phys. Rev. B 34, 3820 (1986),
18. D. Alf`e and M. J. Gillan, Efficient localized basis set for quantum Monte Carlo calculations on condensed matter, Phys. Rev. B 70, 161101(R) (2004),
19. N. D. Drummond, M. D. Towler, and R. J. Needs, Jas trow correlation factor for atoms, molecules, and solids, Phys. Rev. B 70, 235119 (2004),
20. N. D. Drummond and R. J. Needs, Variance minimization scheme for optimizing Jastrow factors, Phys. Rev. B 72, 085124 (2005),
21. C.J. Umrigar, J. Toulouse, C. Filippi, S. Sorella, and R. G. Hennig, Alleviation of the fermion-sign problem by optimization of many-body wave functions, Phys. Rev. Lett. 98, 110201 (2007).